THE INCIDENCE OF CEREBRAL CONTUSIONS IN THE HUMAN: A PHYSICAL MODELING STUDY

David I. Shreiber, Thomas A. Gennarelli*, David F. Meaney
Department of Bioengineering, University of Pennsylvania
*Department of Neurosurgery, Medical College of Pennsylvania/Hahnemann University
Philadelphia, PA

ABSTRACT

Cerebral contusions without overlying skull fracture occur primarily in the frontal and temporal lobes, and are the most frequent clinical evidence of brain damage after closed head injury. In this study, we used physical models of the skull-brain structure to estimate the intracranial strain patterns that were caused by sagittal plane inertial loading. We focused on the changes in intracranial strains as we varied the characteristics of the model (no slip or partial slip interface between skull and brain) and the inertial loading (direction and magnitude).

The findings of these tests indicate that the skull geometry and loading kinetics contribute to the nonuniform strain patterns within a surrogate brain during dynamic loading, and that the skull-brain boundary condition may play a critical role in understanding the high incidence of frontal and temporal lobe contusions observed clinically. In addition, since the data highlight some of the significant factors that affect intracranial strains, they may prove to be a useful guide in the development of more sophisticated techniques to estimate intracranial strains during impact.

CEREBRAL CORTICAL CONTUSIONS are the most frequent evidence of brain damage after head injury (Adams, et al. 1980). Clinically, contusions without overlying skull fracture are most prevalent in the frontal and temporal lobes (Adams, et al., 1985), regardless of the impact direction. The regional preference of cerebral contusions observed clinically has also been recognized in numerous animal models of traumatic brain injury employing direct head impact (Ommaya, et al., 1971; Pudenz and Sheldon, 1946; Ono, et al. 1980; Gurdjian, 1975) and in models using distributed loading conditions (Unterharnscheidt, 1969; Gennarelli, et al., 1979).

The preferential locations of cerebral contusions has prompted numerous theories as to the mechanism of their incidence. These mechanisms are attributed mainly to either cavitation or deformation based damage to the cerebrovasculature. For cavitation injuries to occur, the region of tissue must experience a negative pressure of sufficient magnitude to cause dissolved blood gases to escape and collapse upon return to normal pressure. Several physical model studies have been conducted to characterize the intracranial pressure gradients

during impact, both in water filled and gel filled skull (Gross, 1958; Lubock and Goldsmith, 1980; Gurdjian, 1975). However, the exact threshold for cavitation induced contusion has not been determined.

For deformation based contusions, regional geometric and tissue properties are thought to contribute to the motions and concomitant damage caused by inertial head motions. In some brain regions, investigators have observed that the brain glides easily along the inner skull surface and deforms only slightly (Pudenz and Sheldon, 1946). In other regions, however, the gliding is restricted and strains appear within the brain. Holbourn first demonstrated regional differences in the strains caused by rotational accelerations using gelatin-filled skull sections. These tests simulated impact to the occiput (posterior-anterior sagittal plane rotation), the temples (horizontal rotation), or the ear (coronal rotation) (Holbourn, 1943). Due to changes in the local radius of curvature in the frontal region and the skull shape between the frontal and temporal lobes in the sagittal model, high maximum shear strains were observed near the sphenoid ridge and along the overlying superior margin. Although the strain distribution correlated well with the clinical observations of subdural hematoma along the superior brain surface, it did not exactly match the regional patterns associated with cerebral contusions or intracerebral hematomas.

While the information from Holbourn's studies qualitatively identified shear strains appearing in the brain for rotation simulating occipital impact, several issues need to be studied in order to understand the role of deformation in producing cerebral contusions. These issues include the influence of inertial loading parameters on the intracranial strain patterns, and the sensitivity of strains to the interface between the brain and the skull. This investigation examines the effects of the direction and magnitude of impulsive, sagittal plane, non-centroidal rotation on the resultant intracranial deformations, and studies the role of the boundary condition between the skull and the brain.

METHODS

CONSTRUCTION OF PHYSICAL MODELS - The construction of the physical models used in this study followed the same general procedures employed in previous investigations (Margulies, et al., 1991; Meaney and Thibault, 1991). Adult human skulls (Carolina Biological Supply, Raleigh, NC USA) were cut 1.5 cm lateral to the sagittal midline. Cuts were then made along an interior bony ridge where the tentorium membrane normally attaches in vivo, and the skull was disassembled to insert a surrogate tentorium membrane in the model. This membrane, a polyurethane material, was chosen because its mechanical properties were similar those measured for dura mater (Margulies, 1987). An epoxy resin was used to reassemble the skull completely once the surrogate tentorium was properly placed in position. A surrogate spinal column was inserted into the foramen magnum, with the distal end of the spinal column left open to allow surrogate tissue to exit from the cranial cavity during dynamic loading. The interior of each skull and spinal column was coated with flat white enamel to enhance photographic resolution during high speed filming.

A polymer/resin mix fixed the skull/spinal column assembly inside a cylindrical aluminum can. An optically transparent silicone gel (Sylgard Medical gel, Q7-2218, Dow Corning Inc., Midland, MI, USA) consisting of approximately equal parts of polymer and catalyst was used as the surrogate brain material. This specific gel mixture has mechanical properties similar to primate brain tissue (Blum, 1985; Margulies, 1987). Furthermore, the

gel is self-adherent - a series of layers may be cast to measure deformation in specific anatomic planes of interest. For the model used in this investigation, an initial layer of silicone gel was poured to a level 1.0 cm from the sagittal midline and allowed to cure. An orthogonal black enamel grid (7 mm spacing) was painted on the gel surface and allowed to dry. A second layer of gel was then poured to fill the remainder of the skull section.

As a final step in the construction process, the boundary condition between the silicone gel and inner skull surface was controlled to simulate either a no slip or partial slip condition. If allowed to cure fully, the gel adhered to the inner skull surface and did not move during testing, thereby creating a no slip condition. To create a partial slip between the surfaces, a thin film of mineral oil was inserted between the skull and gel, and mineral oil was used to fill the remainder of the model space.

Just prior to testing, a lucite coverplate was attached to the assembled model; distilled water was injected in the space between the surface of the model and the coverplate. The water creates a pure slip condition at the surface of the model and limits the possible constraining effects of the coverplate. An assembled sagittal section physical model is depicted in Figure 1A.

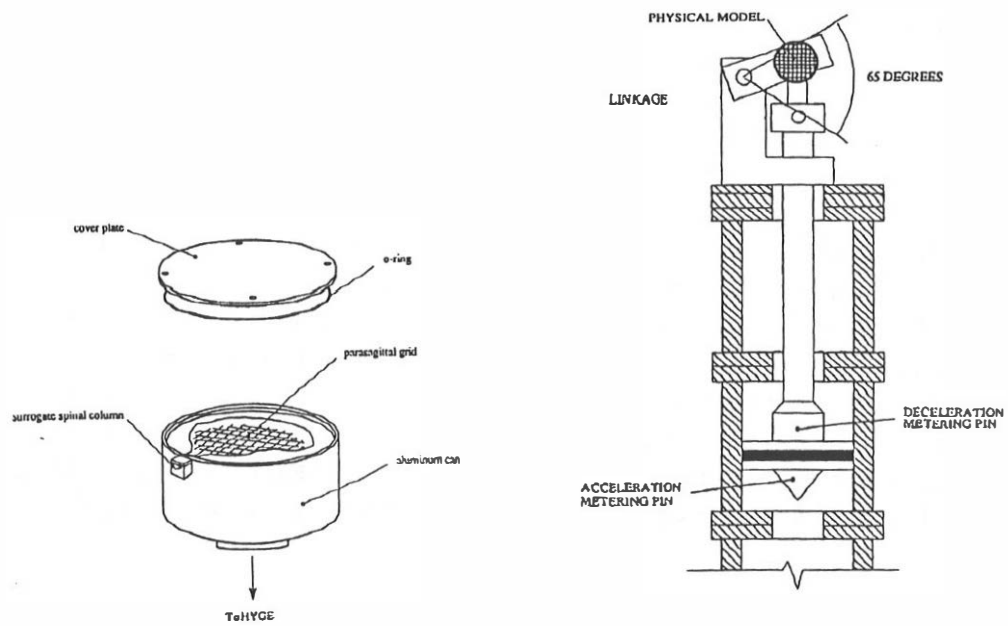

(A) (B)

Fig. 1 - Physical models (A) were subjected to a sagittal plane, non-centroidal rotation by a HYGE device (B). A custom linkage was used to convert linear motion to angular displacement.

ACCELERATION DEVICE - The device used to accelerate the physical model has been used successfully in previous animal and physical model experiments (Gennarelli, et al. 1982; Margulies, et al. 1990; Margulies, 1987; Meaney, 1991). The device consists of a six-inch Bendix HYGE actuator and a linkage assembly which delivers a distributed inertial load to the physical model (Figure 1B). The peak acceleration/deceleration, pulse wave shape, and degree of excursion can be modified as desired. Typically, the acceleration trace is biphasic with a long duration acceleration phase followed by a shorter duration but larger magnitude deceleration pulse. A uniaxial accelerometer (Endevco Instruments, San Juan Capistrano, CA) mounted on the linkage arm was used to record the magnitude of the acceleration pulse in the direction tangent to the angular motion of the model. The acceleration data was amplified, stored on a recorder (Endevco Instruments) and plotted. Later, the acceleration trace was digitized and stored on computer disk.

TEST PROTOCOL - Using the methods outlined above, three models were tested under a series of loading conditions. First, the effect of loading kinetics were evaluated by subjecting a sagittal section model to a noncentroidal sagittal plane rotation. The magnitudes of the rotational acceleration and the rotational velocity were changed between tests but the angular displacement and kinematic path were constant for all tests. Second, the effect of loading direction was investigated by subjecting a model to either an anterior-posterior or posterior-anterior motion. Loading condition kinetics (peak rotational acceleration, peak rotational velocity) were consistent in these tests; only load kinematics were changed. Finally, the influence of skull-brain boundary conditions was studied by testing an adult sagittal section model under sagittal plane loading. Two tests were conducted with a no slip condition at the interface, and two were conducted with mineral oil acting to provide a partial slip between the skull and brain.

DATA ANALYSIS - Deformations of the grid within the gel during dynamic loading were filmed with a high-speed movie camera (HYCAM, Redlake Corp, Morgan Hill, CA, USA) operating at a rate of 6600 frames per second. Individual frames were enlarged and printed, and the grid intersections were digitized (Summagraphics, Seymour, CT, USA). Four independent Green-St. Venant strain tensors were calculated for each grid block (consisting of four nodes of known deformed and undeformed positions) using the relationship:

$$dS^2 - dS_0^{\,2} = 2E_{ij}da_i da_j$$

where dS^2 and $dS_0^{\,2}$ are the distances between two points in the deformed and undeformed frames, respectively, E_{ij} is the Green-St. Venant strain tensor, and da_i is the difference in the i coordinates of the two points in the undeformed frame. The maximum principal strain was then calculated from the Green strain tensor for each triangle (four per grid element) using the relationship:

$$P_1 = \frac{E_{11} + E_{22}}{2} + \sqrt{\left(\frac{E_{11} - E_{22}}{2}\right)^2 + E_{12}^{\,2}}$$

Individual grid blocks in four distinct regions were selected to determine the maximum strain experienced regionally by the cortex: the frontal lobe, posterior to the frontal lobe, the vertex, and the occipital lobe. Selected grid blocks were at least partially within a specific distance (6 mm) from the skull designed to isolate the strain pattern in the cerebral cortex (Figure 2). Maximum principal strain data from each triangle was filtered temporally using a digital smoothing function (Kaleidgraph, Abelbeck Software, USA). The temporally filtered strains for the four triangles within one grid block were then averaged to determine an average maximum principal strain for each grid element. The strain vectors were searched by region for the peak value of maximum principal strain. This value was used to estimate the maximum deformation experienced by the cortex in the appropriate location.

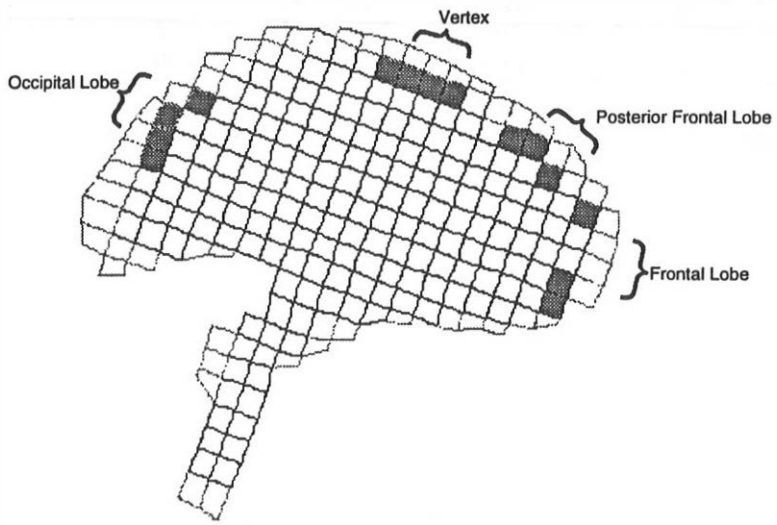

Fig. 2 - Regions analyzed in the physical model (shaded) included the frontal, posterior frontal, and occipital lobes and the vertex. Shaded regions were at least partially within a specific distance (6mm) from the skull.

Additionally, grayscale fringe plots were created to view changes in the intracranial strain profile during impulsive loading. The strain data from all experiments were analyzed to determine the minimum and maximum strains. Each triangle was filled with the appropriate shade of gray, creating a discrete image of the strain pattern for each digitized frame of each experiment. These images were filtered spatially using a Gaussian smoothing filter (Adobe Photoshop, Adobe Systems, Mountain View, CA).

RESULTS

In all, nine tests were conducted to study the influence of kinetic, kinematic, and interfacial conditions on the intracranial strain pattern during inertial loading (Table 1). Acceleration profiles in each test were biphasic, with an initial acceleration pulse followed by a brief, but larger in magnitude, deceleration loading (Figure 3). From these acceleration data, the peak rotational acceleration and peak change in rotational velocity were calculated for each test to characterize the kinetic loading condition of each test.

Model ID	Boundary Condition	Direction of Loading	Tentorium	$\ddot{\theta}_p$ ($\times 10^4\ rad/s^2$)	τ_d (ms)	τ_r (ms)
ASNS15	no slip	Frontal	No	1.39	6.6	3.2
ASNS35	no slip	Frontal	No	3.21	5.8	2.0
ASPS15	partial slip	Frontal	No	1.48	8.6	3.9
ASPS35	partial slip	Frontal	No	2.85	7.1	3.3
ASWT20	no slip	Frontal	Yes	1.24	5.5	2.3
ASWT35	no slip	Frontal	Yes	2.01	5.6	2.6
ASWT65	no slip	Frontal	Yes	3.62	4.9	2.4
ASTO20	no slip	Occipital	Yes	1.42	5.6	2.4
ASTO50	no slip	Occipital	Yes	2.76	5.6	2.2

Table 1 - Experimental protocol including boundary conditions, direction of loading, and magnitude of rotational acceleration. $\ddot{\theta}_p$= rotational acceleration, τ_d = duration of deceleration pulse, τ_r = rise time of deceleration pulse.

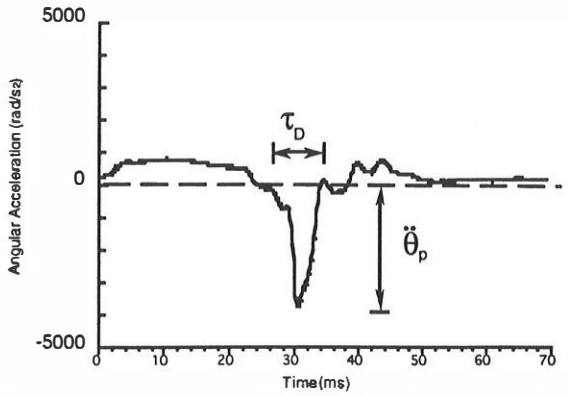

Fig. 3 - The acceleration pulse is characterized by a relatively long acceleration ($\tau \sim 20$ ms) followed by a brief but larger deceleration.

The maximum principal strain at a given location in the model grid pattern followed the inertial loading profile, showing local maximum values in both the acceleration and deceleration phase of the loading period (Figure 4). The overall maximum strains, however, appeared consistently in the deceleration phase of the loading for all regions studied. The maximum strains varied considerably across regions (Figure 5), and were influenced by characteristics of the model and loading conditions used in each test.

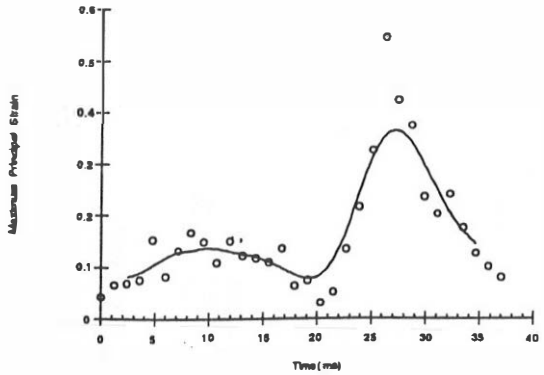

Fig. 4 - Surrogate model response followed the inertial loading input. Shown are the measured and temporally smoothed responses in the frontal region for an adult, sagittal section model with a no slip boundary, subjected to posterior-anterior sagittal plane motion. Maximum principal strain displayed a local maximum during both the acceleration and deceleration phase, with the absolute maximum typically occurring during the deceleration phase.

The maximum principal strain in the surrogate brain increased as the kinetic parameters describing the loading were increased (Figure 5). Although the maximum principal strain was found to occur during the deceleration phase of the loading in all regions studied, the relationship between maximum principal strain and loading parameters was not consistent across the anatomic regions studied. In general, the relationship between principal strains and peak loading conditions was not linear, but increased less as the acceleration was increased.

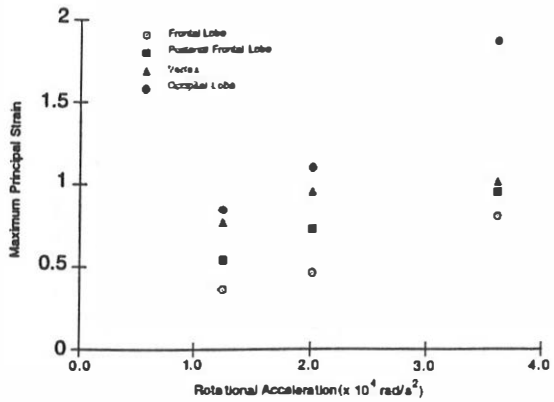

Fig. 5- Maximum principal strain in a brain surrogate varies according to the magnitude of inertial loading as well as location. The magnitude of strain increases nonlinearly with increasing levels of acceleration. The degree of nonlinearity changes with location.

The direction of sagittal plane loading of a physical model using a no slip interface affected the distribution of maximum principal strain in all regions studied(Figure 6). Posterior-anterior motion caused maximum strains in the no slip model to appear along the

vertex and in the occipital region. In comparison, anterior-posterior motion created strain maxima in the vertex and frontal regions. Strains in the occipital region were largest in the posterior-anterior motion tests. Strains in the frontal region were largest for the anterior-posterior motion tests.

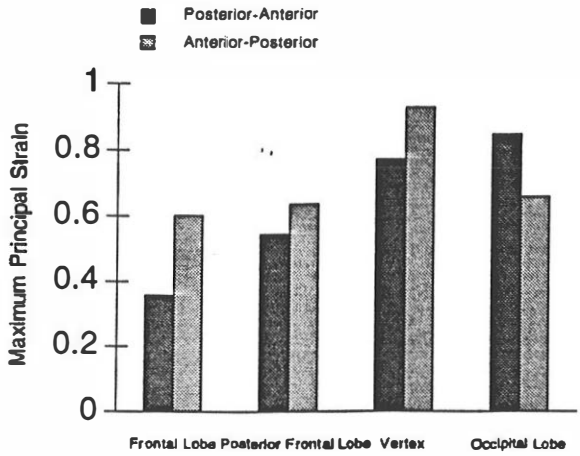

Fig 6 - The direction of loading affected strain in the frontal and occipital regions in a surrogate model constructed with a no slip boundary. Changes in maximum principal strain were not as significant in the vertex or the posterior frontal regions.

The interface condition between the surrogate brain and the inner skull affected both the magnitude and distribution of strain within the brain regions studied (Figure 7). Principal strain in the vertex, posterior frontal, and occipital regions were all lower when a partial slip condition was incorporated into the physical model. In contrast, when the partial slip condition was used, strains in the frontal region increased. The intracranial deformations over time for the no slip and partial slip cases are shown in Figures 8A-B.

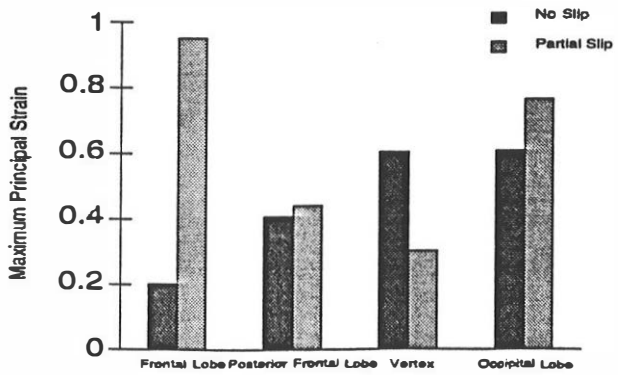

Fig. 7 - Altering the boundary conditions between the surrogate brain and the skull changed the magnitude and the distribution of intracranial strains. A partial slip interface between the surrogate and the skull moved the site of overall maximum strain in the examined cortical regions to the frontal region, in contrast to the occipital region and vertex in models with a no slip interface.

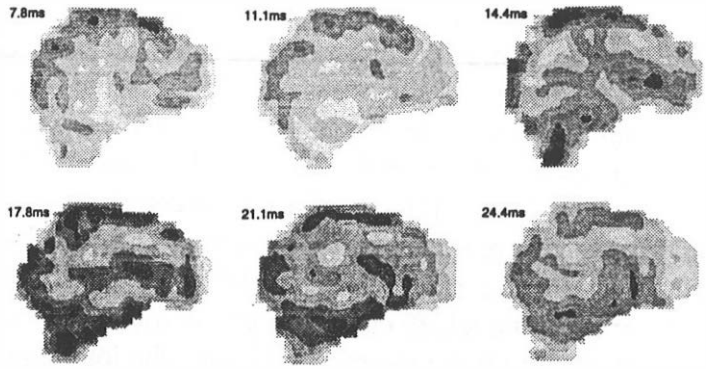

Fig. 8A - Maximum principal strain in the cortex is peak (dark) at the vertex, sphenoidal ridge, and occiput for the no slip model. The grayscale fringe plots portray the temporal and spatial distribution of strain by time.

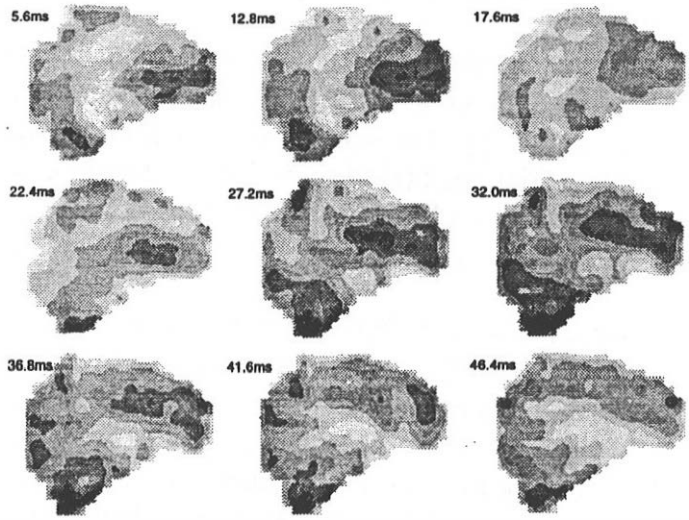

Fig 8B - The strain profile differs for the partial slip case, with peak maximum principal strain (dark) in the cortex appearing in the frontal region.

DISCUSSION

The data from the physical model tests presented in this investigation show that the intracranial strains in regions approximating the cerebral cortex vary considerably among regions in the brain, and that these strain patterns depend both upon the characteristics of the loading conditions and the boundary characteristics used in the physical model. The strain appearing throughout the brain increased nonlinearly with increasing magnitudes of rotational accelerations. Changing the direction of sagittal plane loading affected the distribution of strain in the occipital and frontal cortical brain regions, but did not produce noticeable changes in the strains in either the posterior frontal region or vertex. Finally, adjusting the interface between the brain and the inner skull surface changed the distribution of strain; the site of maximum strain changed from the occipital cortex (no slip) to frontal cortex (partial slip).

The results presented in this study are based on information from surrogate models of the skull brain structure, and therefore should be viewed as estimates of the intracranial deformations. Several steps were taken, however, to ensure that the results were reasonable estimates of the intracranial strain patterns. First, the mechanical properties of the surrogate material were chosen to fall within the range of those reported from human brain tissue (Thibault and Gennarelli, 1984). Future information concerning the variation of the mechanical properties with age, location, and level of strain can be used to evaluate new materials for more accurate modeling efforts. Second, full hemispheres of dried, human skulls were used in the surrogate models to ensure no geometric differences between the physical model and the actual skull brain structure. Finally, the loading conditions were not varied across a broad range of kinematic conditions; the translational motion and degree of noncentroidal rotation were held constant. However, previous studies have demonstrated that that rotational, not translational, acceleration components account primarily for the intracranial strains occurring during impact and impulsive loading (Hodgson and Thomas, 1979; Meaney, et al., 1993).

The results of this investigation correlate well with other similar experimental and computational studies. Holbourn first examined the intracranial strain patterns during sagittal plane rotational loading using gelatin-filled skulls and found high maximum shear strains at the vertex and sphenoidal ridge (Holbourn, 1943). These results were reproduced in a two-dimensional finite element model of sagittal plane acceleration with a no slip interface (Chu, et al., 1993). The FEM results were consistent regardless of the direction of rotational loading.

Similar shear profiles were produced using our method of analysis - elevated shear was evident at the vertex and sphenoidal ridge regardless of loading direction. However, we chose to use maximum principal strain as our estimate of cortical deformation because it is a better representation of the maximum deformation experienced by the surrogate tissue. Figures 8A-B demonstrate that, for the no slip condition, the vertex and sphenoidal ridge, as well as the occipital lobe, experience elevated maximum principal strains for a posterior to anterior motion. The principal strain pattern is reversed, however, for the no slip case when simulating occipital impact - the frontal lobe experiences elevated strains whereas the occipital region experiences diminished strains. Figures 8A-B also illustrate the effects of the partial slip boundary on the temporal distribution of strain. The response of the no slip surrogate model generally follows the acceleration pulse, with little deformation occurring after completion of inertial loading. However, partially decoupling the surrogate brain from the skull results in longer duration responses to both the acceleration and deceleration phases and an overall temporal strain pattern different from the acceleration pulse.

Although a quantitative analysis cannot be made, our results with the pure slip model are similar to the observations made by Pudenz and Sheldon in nonhuman primates. By replacing the skull with a lucite calvarium, these investigators measured the motion of the cortical surface during impact to the frontal, occipital and temporal parietal areas of the skull. For frontal and occipital impacts, the brain glided along the inner surface of the dura at the occipital lobe and the vertex. The brain did not glide in the frontal lobe. Thus, when the head is subjected to rapid rotational acceleration, the interior surface of the frontal bone prevents the brain from following completely. As such, we should expect to see increased

strains at the frontal lobe, where the cortex does not slip across the boundary, and decreased strains at the vertex and occipital regions, where the cortex can rotate along with the brain as a whole in a rigid body fashion. As depicted in Figure 7, the results of the partial slip model agree with these conclusions; the peak maximum principal strain occurred in the frontal lobe and increased over 350% versus the frontal lobe strain in the no slip model for equivalent rotational acceleration. Peak strain decreased versus the no slip case at the vertex (50%) and increased moderately at the occipital lobe (33%).

The presence of excessive strains in the frontal lobe for the partial slip model compare well with clinical and experimental evidence with respect to the preferential location of cerebral contusions. The clinical appearance of "contre-coup" contusions - namely frontal contusions resulting from occipital impact in closed head injury - is a long-observed and well-documented phenomenon (Lindenberg, 1960; Adams, et al., 1980; Adams, et al., 1980; Goggio, 1940; Adams, et al., 1985). This observation has also been made in numerous subhuman primate experimental models involving free impact to the head (Ommaya, 1971; Sano, et al., 1967, Ono, 1980).

In constrained head motions in the Macaque monkey, Gennarelli, et al. (1979) determined thresholds for cerebral contusions and found that frontal and temporal lobe contusions were the predominant type of lesions. Minimal contusions, if any, were observed in the occipital or parietal lobes and were attributed to the skull bending occurring during the loading. Furthermore, the threshold for frontal lobe contusions was lower than for temporal lobe contusions. Frontal lobe contusions first appeared at the anterodorsal durface and the frontal pole, and spread around the frontal tip and extended posteriorly with increasing severity. These injury patterns are most consistent with the maximum principal strain profile from the partial slip model, although there are slight geometric differences between the Macaque monkey and the adult human skull at the frontal lobe. The tip of the frontal lobe is at less of an acute angle in the human. Thus, the anterodorsal surface of the monkey correlates with the anterior pole of the human.

The results of this investigation have implications concerning the future of experimental and computational modeling of traumatic head injury. The dramatic effect of changing boundary conditions from no slip to partial slip on the intracerebral strain pattern, and the excellent correlation of that strain pattern with clinical and experimental observations of contusions, suggests that a more extensive series of models needs to be tested under the partial slip conditions. These tests will include studying the role of loading direction, duration, and geometric constraints on overall strain response and, in particular, the strains appearing in the cortical regions. Furthermore, future studies should concentrate on quantifying the degree of slip during angular acceleration loading, including the effects of the bridging veins on the degree of slip over time. These boundary conditions must also be incorporated into current finite element models to achieve a better understanding of intracranial dynamics during traumatic loading.

ACKNOWLEDGMENTS

Funds were provided by the Centers for Disease Control R49/CCR 304684 and the National Institutes of Health NS-08803.

REFERENCES

Adams, J., D. Doyle, et al. The contusion index: a reappraisal in human and experimental non-missile head injury. *Neuropathology and Applied Neurobiology* **11**: (1985)299-308.

Adams, J., D. Graham, et al. Brain damage in fatal non-missile head injury. *Journal of Clinical Pathology* **33**: (1980)1132-1145.

Blum, R. and L. Thibault. In-vivo indentation of the cerebral cortex. *35th ACEMB*, Chicago, IL, (1985).

Chu, C., M. Lin, et al. Finite element analysis of cerebral contusion. *Journal of Biomechanics* **27**(2): (1993)187-194.

Gennarelli, T., J. Abel, et al.. Differential tolerance of frontal and temporal lobes to contusion induced by angular acceleration. *23rd Stapp Car Crash Conference*, 563-586, 1979.

Gennarelli, T., L. Thibault, et al. Diffuse axonal injury and prolonged coma in the primate. *Annals of Neurology* **12**: (1982)564-574.

Goggio, A. The mechanism of contre-coup injury. *Journal of Neurology, Neurosurgery, and Psychiatry* **4**: (1941)11-22.

Gross, A. Impact thresholds of brain concussion. *Journal of Aviation Medicine* **29**: (1958)625-732.

Gurdjian, E. and E. Gurdjian. *Impact Head Injury - Mechanical, Clinical, and Preventive Correlations*. Springfield, IL, Charles Thomas (1975).

Hodgson, V. and L. Thomas. Acceleration Induced Shear Strains in a Monkey Brain Hemisection. *23rd Stapp Car Crash Conference* : (1979)485-497.

Holbourn, A. Mechanics of head injuries. *The Lancet* : (1943)438-441.

Lubock, P. and W. Goldsmith. Experimental cavitation studies in a model head-neck system. *Journal of Biomechanics* **13**: (1980)1041-1052.

Margulies, S. Biomechanics of traumatic coma in the primate. University of Pennsylvania, (1987).

Margulies, S., L. Thibault, et al. Physical model simulations of brain injury in the primate. *Journal of Biomechanics* **23**(8): (1990)823-836.

Meaney, D. The Biomechanics of Acute Subdural Hematoma in the Subhuman Primate and Man. University of Pennsylvania, (1991).

Meaney, D., K. Thibault, et al. Experimental investigation of the relationship between head kinematics and intracranial tissue deformation. *Advances in Bioengineering* **24**: (1993)8-11.

Ommaya, A., R. Grubb Jr., et al. Coup and contre-coup injury: observations on the mechanics of visible brain injuries in the rhesus monkey. *Journal of Neurosurgery* **35**: (1971)503-516.

Ono, K., A. Kikuchi, et al. Human head tolerance to sagittal impact reliable estimation deduced from experimental head injury using subhuman primates and human cadaver skulls. *24th Stapp Car Crash Conference*, Society of Automotive Engineers (1980).

Pudenz, R. and C. Sheldon. The lucite calvarium – a method for direct observation of the brain. II. Cranial trauma and brain movement. *Journal of Neurosurgery* **3**: (1946)487-505.

Thibault, L. and T. Gennarelli. Biomechanics of Craniocerebral Trauma. *C.N.S. Trauma Status Report*, Bethesde, MD, NIH (1984).

Unterharnscheidt, F. and L. Higgins. Traumatic lesions of brain and spinal cord due to nondeforming angular acceleration of the head. *Texas Reports on Biology and Medicine* **27**(1): (1969)127-166.